



Impacts of Arctic sea ice loss on global ocean circulations and interbasin ocean heat exchanges

Shouwei Li¹ · Wei Liu¹

Received: 1 November 2021 / Accepted: 2 March 2022 / Published online: 19 March 2022
© The Author(s), under exclusive licence to Springer-Verlag GmbH Germany, part of Springer Nature 2022

Abstract

The Arctic sea ice loss during the past several decades plays an important role in driving global climate change. Herein we explore the effects of Arctic sea ice loss on global ocean circulations and ocean heat redistribution. We find that in response to Arctic sea ice loss, oceans are taking up heat from the atmosphere via sensible and latent heat fluxes mainly in the subpolar North Atlantic. Meanwhile, Arctic sea ice loss induced ocean circulation changes could redistribute the taken heat, which, however, is timescale-dependent. Within a decade after Arctic sea ice loss, the Atlantic meridional overturning circulation (AMOC) is little altered such that most of the taken heat is locally stored in the Atlantic. On a multidecadal to centennial timescale, the AMOC decelerates redistributing the heat to other basins through interbasin ocean heat exchanges. In the Indo-Pacific Ocean, an anomalous ocean circulation is generated manifesting an abnormal northward flow near the surface, which imports about one-third of the redistributed heat from the Atlantic, via the Southern Ocean and into the Indian Ocean. Meanwhile, the Indonesia Throughflow weakens giving rise to an anomalous ocean heat transport from the Indian to Pacific Ocean. As a result, both Indian and Pacific Oceans are warmed on a multidecadal to centennial timescale. The Arctic sea ice loss also induces a “mini” global warming with a pronounced lower to middle tropospheric warming in the Southern Hemisphere. Accordingly, the Southern Hemisphere westerly winds poleward intensify to modulate the Deacon Cell and residual MOC in the Southern Ocean. Along with the ocean circulation changes and associated variations in ocean heat transport across the boundary between the Southern Ocean and Atlantic/Indo-Pacific Oceans, two-thirds of the ocean heat imported from the Atlantic remains in the Southern Ocean.

1 Introduction

Satellite observations depict that Arctic sea ice has declined rapidly during the past several decades (Fig. 1a–c; e.g., Ding et al. 2017; Stroeve et al. 2012), which has been attributed to greenhouse gases (GHGs) increases (e.g., Vihma 2014; Park et al. 2015); and internal climate variability (Li et al. 2018). Arctic sea ice loss has been suggested as a key factor in driving climate changes in northern mid- and high-latitudes. For instance, over the Arctic Ocean, sea ice retreat opens ocean and hence modulates the atmosphere–ocean exchanges, leading to an increase in atmospheric moisture (Rinke et al. 2013) as well as the heat flux from oceans to the atmosphere (e.g., Francis et al. 2009; Overland and Wang 2010); . The sea ice induced atmospheric moisture increase

and low tropospheric warming can extend to the Northern Hemisphere mid- and high-latitudes (Deser et al. 2010; Screen and Simmonds 2010); where the meridional gradient of low-level atmosphere temperature weakens (Francis et al. 2009). As a result, North Pacific storm tracks migrate southward (Oudar et al. 2017), along with a dipole-like sea level pressure change that resembles the negative phase of the North Atlantic Oscillation (Peings and Magnusdottir 2014).

The effect of Arctic sea ice loss does not restrict to northern mid- and high-latitudes but extends over the globe (Liu and Fedorov 2019). Chiang and Bitz (2005) perturbed high latitudes ice cover in a slab ocean model and found that rapid cooling and drying air is generated over the entire high- and mid-latitudes and subsequently extend to Pacific and Atlantic low latitudes. Later, Deser et al. (2015) analyzed the effect of Arctic sea ice loss in both slab-ocean and coupled atmosphere–ocean model simulations and found that the ice effect is mainly confined in the northern hemisphere with warming in the high latitudes in the absence of ocean dynamics. However, when ocean dynamics are considered,

✉ Shouwei Li
sli227@ucr.edu

¹ Department of Earth and Planetary Sciences, University of California Riverside, Riverside, CA, USA

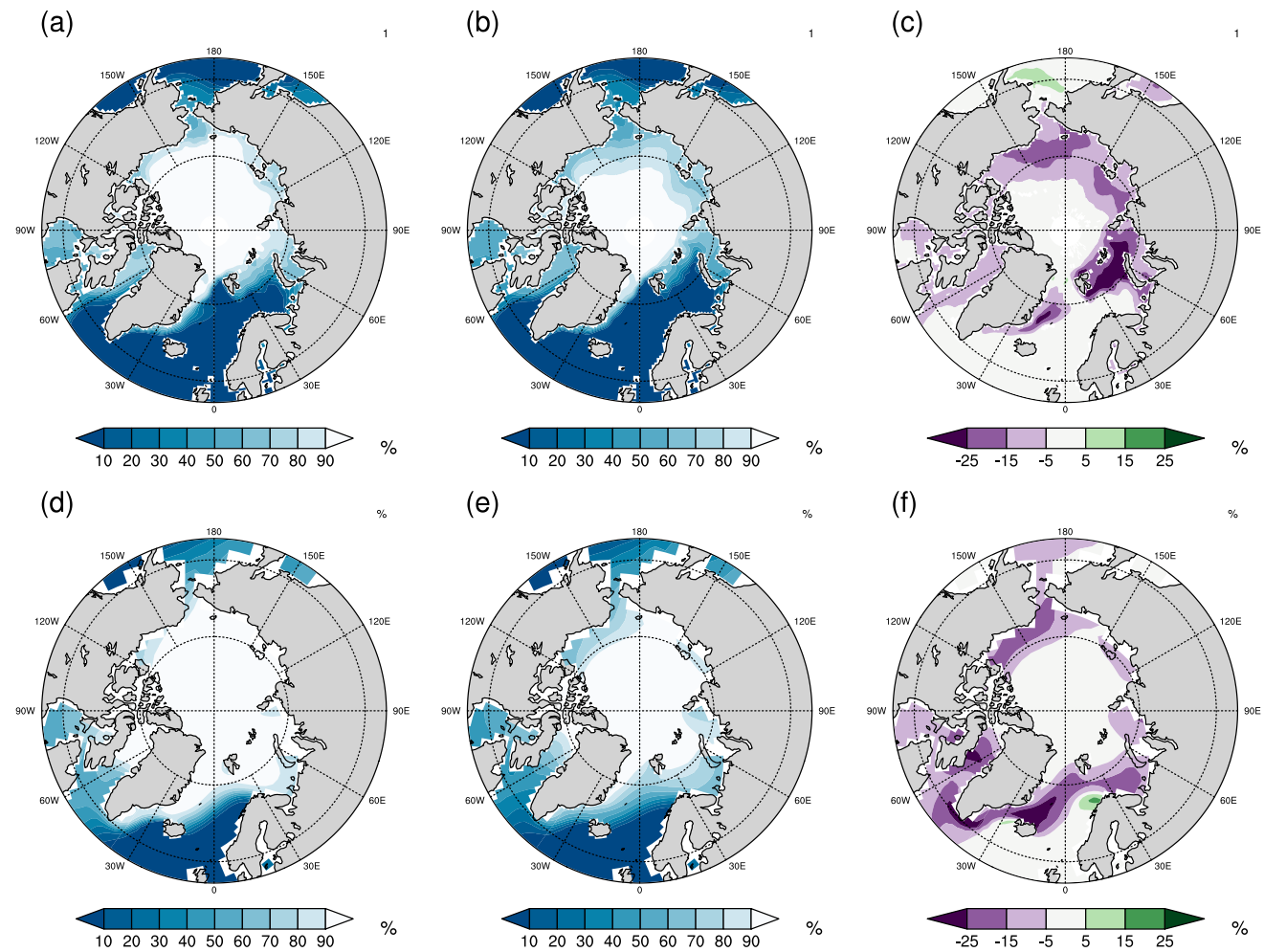


Fig. 1 Observed annual mean of Arctic sea ice concentration from NSIDC during **a** 1980–1989 and **b** 2006–2015 and **c** the difference between the two periods given by **b**–**a**. Simulated Arctic sea ice

concentrations in **d** the control run, **e** the ensemble mean of the last 100 years of the Arctic sea ice perturbation simulation and **f** the difference between the two given by **e**–**d**

the effect of Arctic sea ice loss can extend to tropics or even Antarctic, prompting a global warming except the low stratosphere in high latitudes in both hemispheres. The difference between slab-ocean and coupled atmosphere–ocean model simulations indicates the importance of ocean circulation to global climatic impacts of Arctic sea ice loss. Particularly, as a density-driven ocean circulation that is related to deep water formation in the subpolar North Atlantic, the Atlantic meridional overturning circulation (AMOC), has drawn the most attention (Liu et al. 2017). It has been reported that Arctic sea ice loss can modulate AMOC variations through either haline (Jungclaus et al. 2005; Sévellec and Fedorov 2015); or thermal (Levermann et al. 2007) processes. Conducting an adjoint sensitivity analysis with an ocean model, Sévellec et al. (2017) suggested that both thermal and haline processes operate in contributing to the generation of buoyancy anomalies and a subsequent AMOC weakening. This result was supported by later studies based on fully coupled

climate model simulations (Sun et al. 2018; Liu et al. 2019; Li et al. 2021; Liu and Fedorov 2021).

The AMOC slowdown, on the other hand, can modulate the ocean heat uptake, transport and storage in the Atlantic. Previous GHGs warming (e.g., Shi et al. 2018; Liu et al. 2020); and freshwater hosing (e.g., Zhang and Delworth 2005; Jackson and Wood 2020); experiments showed that a weakened AMOC causes a reduced northward ocean heat transport in the Atlantic, which results in an oceanic heat divergence and temperature cooling to the south of Greenland. The surface temperature cooling, furthermore, promotes ocean heat uptake in the subpolar North Atlantic region (e.g., Drijfhout 2015; Gregory et al. 2016; Ma et al. 2020; Marshall and Zanna 2014; Shi et al. 2018; Winton et al. 2013).

Meanwhile, as a part of global conveyor belt, the AMOC can also play a role in modifying the ocean heat content in ocean basins beyond the Atlantic (Garuba and Klinger 2016).

Triggered by a perturbation in the North Atlantic Deep Water formation to decelerate the AMOC, the subsequent signals propagate in form of an equatorward Kelvin wave along the western boundary in the Atlantic (Kawase 1987; Johnson and Marshall 2002; Zhang 2010); . They further travel across the equator eastwardly and propagate poleward along the eastern boundary (e.g., Cessi et al. 2004; Huang et al. 2000; Sévellec and Fedorov 2013; Sun et al. 2020). The Kelvin wave leads to abnormal meridional geostrophic transport with opposite signs in the Indo-Pacific and Atlantic Oceans by altering the zonal difference of interface depth, hence resulting in an abnormal northward ocean circulation near the surface at the boundaries with the Southern Ocean (Sun et al. 2020). Also, the Indonesian Throughflow (ITF) weakens due to a decreased pressure gradient between the Indian Ocean and Pacific (Sun and Thompson 2020), which further adjusts the interbasin exchange between the Pacific and Indian Oceans (e.g., Hu and Sprintall 2017; Lee et al. 2015).

To summarize, Arctic sea ice loss has been suggested to induce an AMOC slowdown that can reshape the ocean heat content in ocean basins under GHGs warming and freshwater hosing scenarios. Nevertheless, it remains unclear that how Arctic sea ice loss, via changing the AMOC, governs global ocean heat uptake and heat redistribution between ocean basins. This is because, under GHGs warming, changes in Arctic sea ice and the AMOC happen concurrently such that it is hard to disentangle their effects on global ocean heat uptake and redistribution. Moreover, global ocean heat content anomalies could be attributed more to direct surface warming such that the effect of ocean circulation change is overwhelmed (Garuba and Klinger 2016). The freshwater hosing, on the other hand, is usually discussed in the context of paleo-climate (e.g., Yang et al. 2015a) in which large freshwater discharges due to past icesheet melts cause a strong AMOC weakening (McManus et al. 2004). The impact of on-going and future icesheet melts that mainly come from Greenland in the Northern Hemisphere, however, is of secondary importance to the on-going and future AMOC changes (Bakker et al. 2016).

In this study, we will combine observations and climate model simulations to explore the impacts of Arctic sea ice loss on global ocean circulations, heat uptake and redistribution. The structure of the study is as follows. In Sect. 2, we introduce the observations, perturbation experiment and ocean heat budget analysis. We present the main results in Sect. 3, and the paper's conclusion and discussion in Sect. 4.

2 Methods

2.1 Observations

We use observations of Arctic sea ice concentration and extent from the National Snow and Ice Data Center

(NSIDC). The observations are produced based on two brightness temperature data sets: one is derived from Nimbus-7 Scanning Multichannel Microwave Radiometer (SMMR) processed at NASA Goddard Space Flight Center (GSFC), and the other is derived from Special Sensor Microwave/Imagers (SSM/Is) and Special Sensor Microwave Imager/Sounder (SSMIS) processed at the NSIDC. The NSIDC data include monthly averaged sea ice concentration and extent since 1978 October, wherein the sea ice concentration is provided in the polar stereographic projection at a grid cell of 25 km × 25 km. The sea ice extent is defined as the ocean area with sea ice concentration at least 15%. In this study, we compare the annual mean sea ice concentrations over the Arctic area during two periods of 1980–1989 and 2006–2015 and adopt the difference between these two periods (Fig. 1a–c) as the benchmark for the following experimental setup. Particularly, the observed annual sea ice extent indicates a decrease by about 14% from 1980–1989 to 2006–2015, with the maximum seasonal decrease occurring in September by about 33% (Fig. S1).

2.2 Model experiment

We use the Community Earth System Model (CESM) version 1.0.4 from the National Center for Atmospheric Research that includes the Community Atmosphere Model version 4 [CAM4; Neale et al. (2010)], the Community Land Model, version 4 [CLM4; Lawrence et al. (2012)], the Parallel Ocean Program, version 2 [POP2; Smith et al. (2010)], and the Community Ice Code, version 4 [CICE4; Holland et al. (2012)]. The atmosphere and land components use a T31 spectral truncation with 27 vertical layers in the atmosphere. The ocean and sea ice components use an irregular horizontal grid with a nominal ~ 3° resolution but is significantly finer (~ 1°) close to Greenland and in the Arctic Ocean. There are 60 vertical layers in the ocean. The ocean model employs a variable coefficient in the Gent–McWilliams eddy parameterization (Gent and McWilliams 1990), which allows the model to simulate an appropriate ocean response to wind change as indicated by eddy-resolving models (Gent and Danabasoglu 2011).

We conduct ensemble perturbation experiments based on the CESM preindustrial control run to replicate the observed Arctic sea ice loss during the past several decades. To achieve this goal, we lower the albedo of bare and ponded sea ice and snow cover on ice over the Arctic Ocean in the model sea ice component. We have tested different sea ice/snow reflectivity and emissivity parameters to achieve an Arctic sea ice loss. Herein we adopt one of the simulations that depicts the observed Arctic sea ice best (Fig. 1d–f) in which the standard deviation parameters of bare and ponded sea ice (R_{ice} and R_{pnd}) are changed from 0 to – 2 and the single scattering albedo of snow is reduced by 9% for all

spectral bands. Further, to diminish the effect of internal variability, we also slightly modify the initial condition of the model atmosphere component to obtain 10 ensemble members. All of ensemble members are performed with the “best” sea ice/snow reflectivity and emissivity parameters and last for 200 years. We mainly present the results from the ensemble mean in the following parts. For example, the ensemble mean shows that the annual Arctic sea ice area has been decreased by about 14% in the last 100 years of the simulation compared with the control run, which is close to the observed Arctic sea ice loss from 1980–1989 to 2006–2015. The seasonal Arctic sea ice reduction also peaks in September, by about 34% relative to the control run (Fig. S1).

2.3 Ocean heat budget analysis

We use the basin-integrated full-depth oceanic heat budget as below:

$$\iiint \rho_0 C_p \frac{\partial \theta}{\partial t} dx dy dz + \iiint \rho_0 C_p [\nabla \cdot (\mathbf{v} \theta + D)] dx dy dz = \iint (NSHF) dx dy \quad (1)$$

where ρ_0 is seawater density, C_p is the specific heat of sea water and θ is potential temperature of sea water. $NSHF$ denotes net surface heat flux, which is the sum of radiative shortwave (SW) and longwave (LW) fluxes, turbulent sensible (SH) and latent (LH) heat fluxes as well as the heat flux due to snow/sea ice formation and melt (IMS). ∇ and \mathbf{v} are three-dimensional gradient operator and velocity, and $\mathbf{v} = \bar{\mathbf{v}} + \mathbf{v}^*$. D denotes diffusion and other sub-grid processes. The x and y integrals are from the western to eastern boundary and from the southern to northern boundary for individual basins (the x integral is contour integral at the latitude of the Drake Passage). The z integral is from ocean bottom to ocean surface.

Based on Eq. (1), the ocean heat content (OHC) is defined as:

$$OHC = \iiint \rho_0 C_p \theta dx dy dz \quad (2)$$

The OHC tendency as ocean heat storage (OHS) is defined as:

$$OHS = \frac{\partial}{\partial t} OHC = \frac{\partial}{\partial t} \iiint \rho_0 C_p \theta dx dy dz \quad (3)$$

The ocean heat uptake (OHU) is defined as:

$$OHU = \iint (NSHF) dx dy \quad (4)$$

The interbasin oceanic heat transport (OHT) is defined as

$$OHT = \iint \rho_0 C_p (\bar{\mathbf{v}} \cdot \theta + \mathbf{v}^* \cdot \theta + D) dx dz = \overline{OHT} + OHT^* + OHT^d \quad (5)$$

where $\overline{OHT} = \iint \rho_0 C_p \bar{\mathbf{v}} \cdot \theta dx dz$, $OHT^* = \iint \rho_0 C_p \mathbf{v}^* \cdot \theta dx dz$ and $OHT^d = \iint \rho_0 C_p D dx dz$.

Equation (5) shows that the interbasin ocean heat transport (OHT) at each ocean boundary, can be induced by Eulerian-mean flow (\overline{OHT}), eddies (OHT^*) and diffusion (OHT^d) (Yang et al. 2015b).

For each basin, the net meridional oceanic heat transport is calculated as the sum of the OHT across the boundaries of the basin. As a result, the basin-integrated oceanic heat budget by Eq. (1) can be written as

$$OHS = OHU - (OHT_{north} - OHT_{south}) \quad (6)$$

where OHT_{north} and OHT_{south} denote the OHT s at the northern and southern boundaries of each ocean basin. Note here, OHT in Eq. (5) is defined as meridional ocean heat transport since it will be mostly discussed in the following

sections, whereas the OHT between the Indian and Pacific Oceans is zonal, which should be otherwise defined as $OHT = \iint \rho_0 C_p (\bar{\mathbf{v}} \cdot \theta + \mathbf{v}^* \cdot \theta + D) dy dz$. Accordingly, the OHT at the eastern boundary of the Indian Ocean (or at the western boundary of the Pacific Ocean) should be considered. For simplicity, we keep the expressions of Eqs. (5) and (6) and add the note here.

In this study, Arctic sea ice loss induced changes in the ocean heat budget in the perturbation experiment are defined as:

$$\Delta OHS = \Delta OHU - (\Delta OHT_{north} - \Delta OHT_{south}) \quad (7)$$

ΔOHS can be represented by the change in the OHC tendency [$\Delta Tr(OHC)$], which is defined as

$$\Delta Tr(OHC) = Tr(OHC) - Tr(OHC_{ctrl}) \quad (8)$$

where Δ refers to the differences between the perturbation experiment and the control run simulation and $Tr(OHC)$ and $Tr(OHC_{ctrl})$ refer to the OHC trends in the Arctic sea ice perturbation simulation and the preindustrial control run. $Tr(OHC_{ctrl})$ could be associated with the temperature trend drift in the control, which might be small but is not necessary to be zero. Equation (7) indicates that the ocean heat storage anomaly induced by Arctic sea ice loss within one ocean basin is determined by the ocean heat uptake via atmosphere–ocean interface and the net ocean heat transports by ocean circulations, eddies and diffusion across the boundaries of the basin.

We further decompose the Eulerian mean OHT change ($\overline{\Delta OHT}$) into the circulation anomaly driven component ($\overline{\Delta OHT}_{v'}$) and the temperature anomaly driven component ($\overline{\Delta OHT}_{\theta'}$). Specifically,

$$\overline{\Delta OHT}_{v'} = \iint \rho_0 C_p \bar{v}' \theta_0 dx dz \quad (9)$$

where \bar{v}' denotes the change in monthly Eulerian-mean velocity and θ_0 is the monthly climatological ocean temperature in the control run.

$$\overline{\Delta OHT}_{\theta'} = \iint \rho_0 C_p \bar{v}_0' \theta' dx dz \quad (10)$$

where θ' denotes the change in monthly ocean temperature and \bar{v}_0 is the monthly climatological Eulerian-mean velocity in the control run.

3 The fast response due to regional atmosphere–ocean interactions

We first examine the changes in Arctic sea ice and ocean circulations in our Arctic sea ice perturbation experiment. In response to the reduced albedo, Arctic sea ice shows a rapid decrease of up to $2 \times 10^{12} \text{ m}^2$ in area and is up to 2 m in thickness within the first 5 years of the experiment (Fig. 2a; Fig. S3). The rapid Arctic sea ice retreat produces a surface freshwater input to the northern hemisphere oceans up to about 0.2 Sv (e.g., Li and Fedorov 2021), which is within the range of previous housing experiments (e.g., Jackson and Woods 2020). Compared to this fast sea ice retreat, changes in ocean circulations are much slower and related to the propagation of sea ice induced buoyancy signals (Liu et al. 2019). During the first 10 years, most of sea ice induced buoyancy signals are confined within central Arctic Ocean and the Barents Sea. After that, these buoyancy anomalies propagate downstream extending to the North Atlantic deep convection regions, which suppress the formation of North Atlantic Deep Water there (Sévellec et al. 2017; Liu et al. 2019); and lead to an AMOC weakening on multi-decadal timescales. By the end of the perturbation experiment, the decline of the AMOC is about 6 Sv (1 Sv = $10^6 \text{ m}^3/\text{s}$), manifesting a drop about one-third of the AMOC strength in pre-industrial control run (Fig. 2b).

Along with the fast sea ice but slow AMOC responses, ocean heat uptake and interbasin ocean heat exchange exhibit distinct evolution patterns on different timescales. Within the first 10 years of the experiment when the AMOC strength is rarely modified by Arctic sea ice loss, changes in oceanic heat are mainly driven by atmospheric processes and constrained in the Atlantic basin. Specifically, Arctic sea ice loss allows more incoming solar radiation to warm

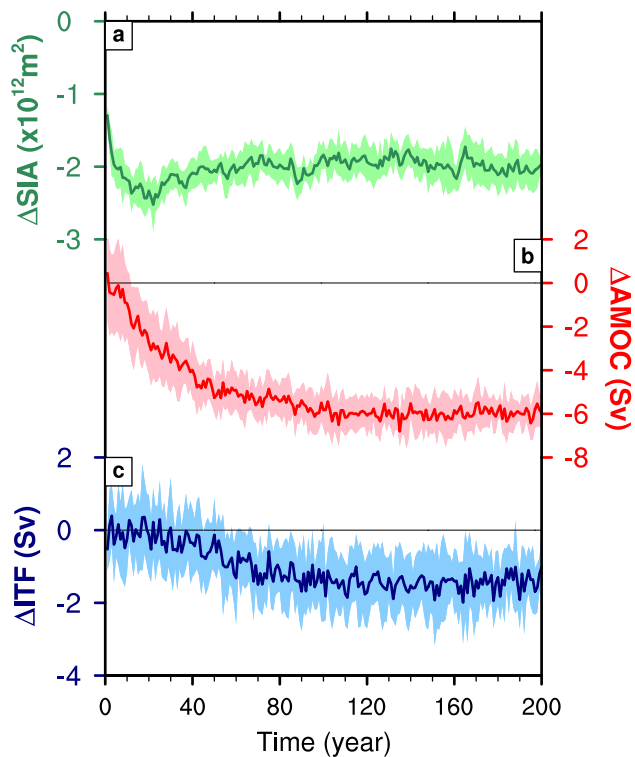


Fig. 2 Changes in **a** Arctic sea ice area (ensemble mean, dark green; ensemble spread, light green), **b** AMOC strength (ensemble mean red; ensemble spread, pink) and **c** ITF strength (ensemble mean, dark blue; ensemble spread, blue) in the Arctic sea ice perturbation simulation. The ensemble spread is calculated as one standard deviation of the 10 ensemble members of the perturbation simulation

the lower to middle troposphere in the Northern Hemisphere (Fig. S4a). The atmospheric warming pattern here is consistent with previous studies with atmosphere-only simulations (e.g., Deser et al. 2015), thus identifying the dominant role of atmospheric processes in the fast response to Arctic sea ice loss.

Besides the warming in the atmosphere, Arctic sea ice loss can affect ocean surface heat fluxes. In the North Atlantic, we find that the Arctic sea ice loss promotes a net surface heat flux ($NSHF$) in the first 10 years of the perturbation experiment (Fig. 3a). The intensified $NSHF$ is mainly attributed to the increase of surface turbulent heat fluxes (sensible plus latent heat fluxes) as a result of atmospheric warming (Fig. S5a; also c.f. Screen et al. (2013), Oudar et al. (2017)). Meanwhile, the altered ice melting and formation create a positive anomaly of surface heat flux to the south of Greenland (Fig. S5c) through a net latent heat release after the phase changes over seasons. The sea ice loss also leads to an open ocean, allowing more solar radiation absorbed by the ocean. Though solar warming is partially compensated by longwave cooling at ocean surface, the net surface radiative (shortwave plus longwave) energy flux anomaly is positive over the

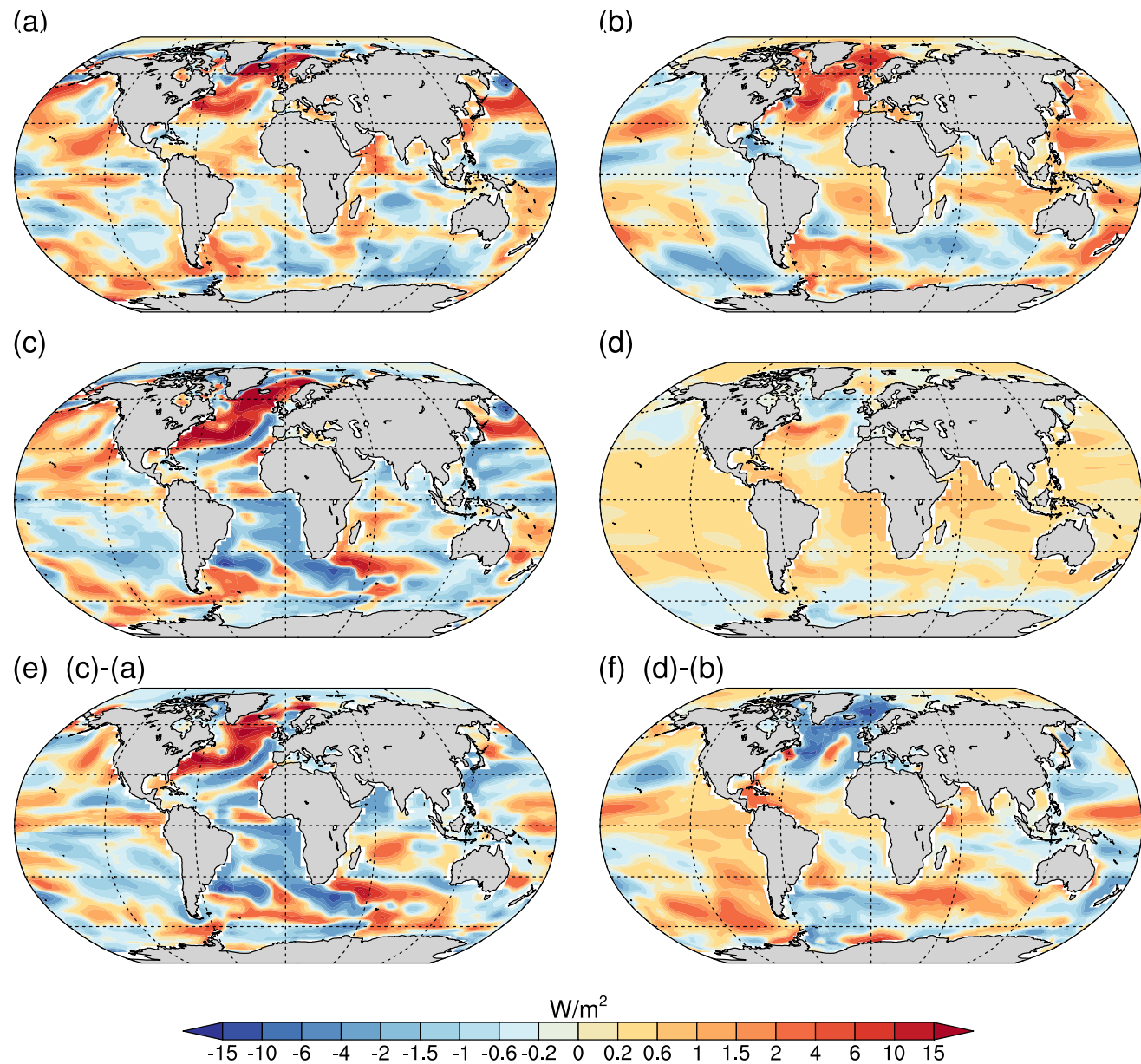


Fig. 3 (Left column) Arctic sea ice loss induced changes (relative to the control) in annual mean NSHF over **a** the first 10 years and **c** the later 100 years for the ensemble mean of the Arctic sea ice perturba-

tion simulation as well as **e** the difference between the two periods given by **c-a**. (Right column) As in the left column but changes in the full depth integrated ocean heat storage

Labrador Sea (Fig. S5b), indicating that heat is entering the ocean in the North Atlantic in response to Arctic sea ice loss.

On the other hand, the AMOC is little modified within the first 10 years. With a neglectable AMOC change, the meridional ocean heat transports across the boundary between the Atlantic and Southern Oceans ($\sim 32^\circ$ S) and the boundary between the Atlantic and Arctic Oceans ($\sim 65^\circ$ N) are also little altered (Fig. 4a). As a result, changes in the net *OHT* are much smaller than those in the *OHU* over the Atlantic basin, which suggests a dominant role of atmosphere–ocean

interactions in modifying the Atlantic Ocean heat storage on a decadal time scale in response to Arctic sea ice loss.

The neglectable changes in *OHT* across the Atlantic boundaries indicate that the Atlantic neither exports heat into nor imports heat from other ocean basins. Hence most of the taken heat from the atmosphere is stored locally contributing to the *OHS* increase in the Atlantic. Herein we quantify the change rate of the integrated *OHC* over the whole Atlantic basin and find that the Atlantic Ocean has gained about 0.07 PW from the atmosphere during the first 10 years of the experiment (Fig. 4a). In another word,

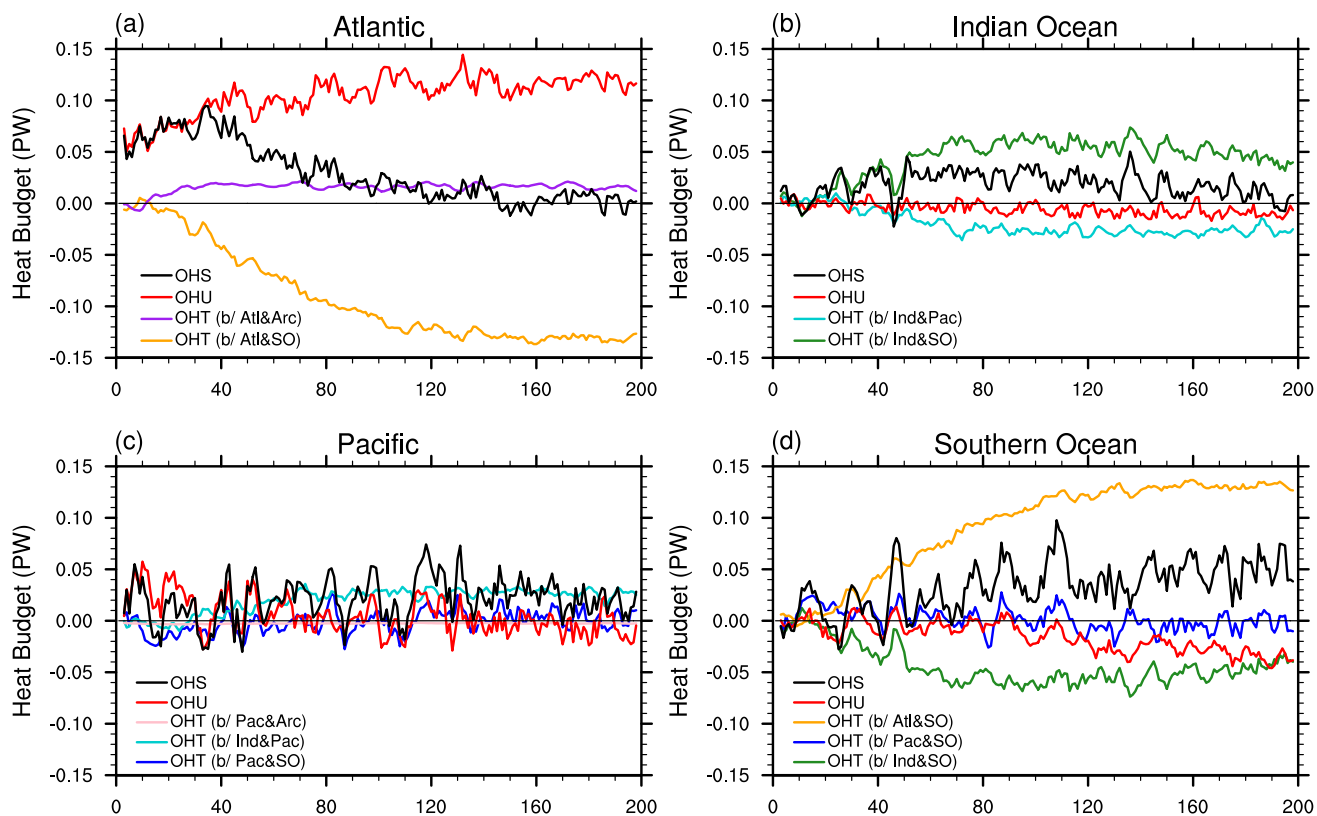


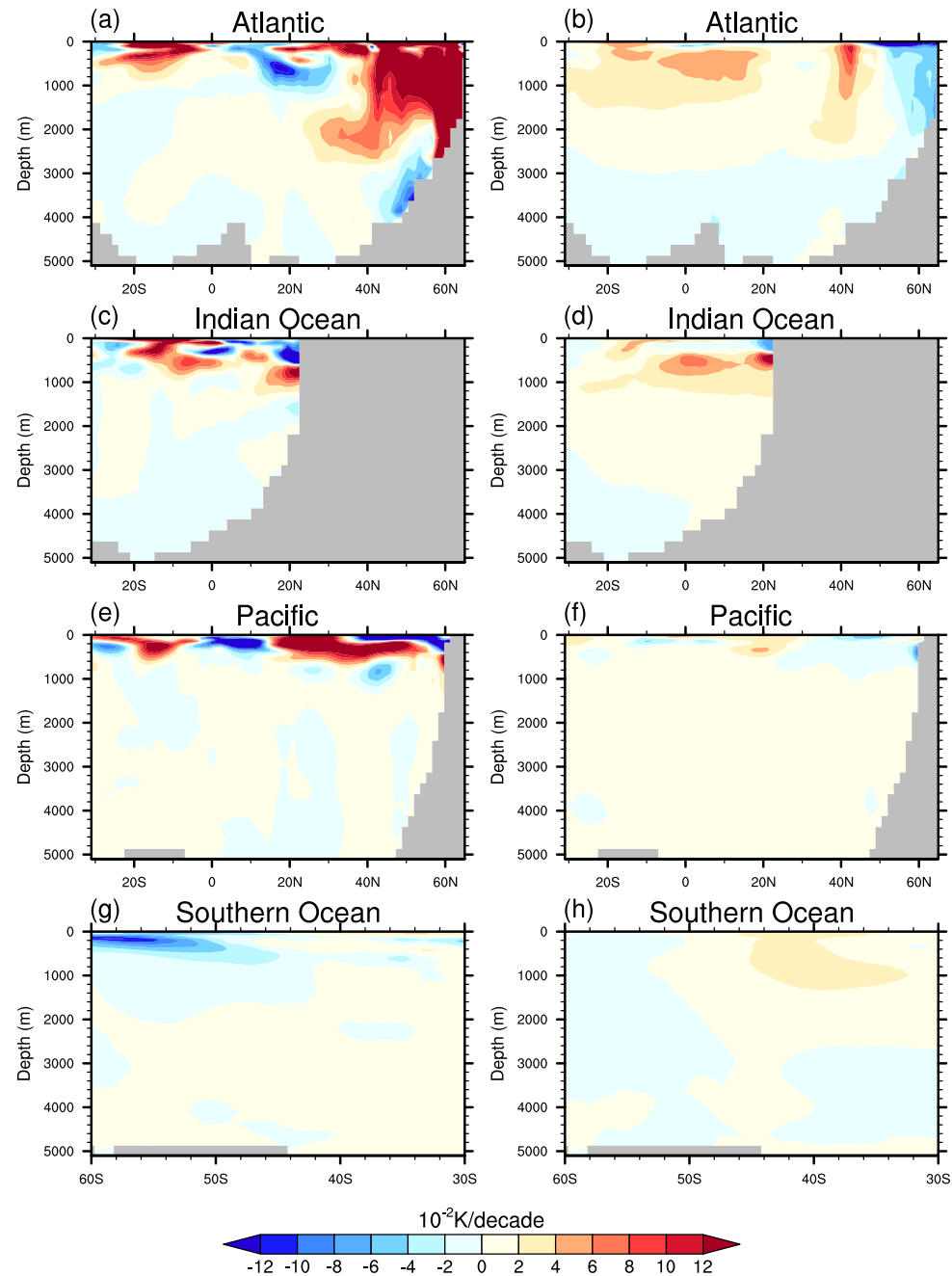
Fig. 4 **a** Arctic sea ice loss induced changes (relative to the control) in annual mean ocean heat budget terms in the Atlantic: OHS (black), OHU (red), OHT at the Atlantic and Arctic boundary (purple), and at the Atlantic and Southern Ocean boundary (gold). **b** Arctic sea ice loss induced changes in annual mean ocean heat budget terms in the Indian Ocean: OHS (black), OHU (red), OHT at the Indian Ocean and Pacific boundary (cyan), and OHT at the Indian Ocean and Southern Ocean boundary (green). **c** Arctic sea ice loss induced changes in annual mean ocean heat budget terms in the Pacific: OHS (black), OHU (red), OHT at the Pacific and Arctic boundary (pink), and OHT at the boundary of the Pacific and Southern Oceans (blue),

and OHT at the boundary of the Indian and Pacific Oceans (cyan; same as the cyan curve in **b**). **d** Arctic sea ice loss induced changes in annual mean ocean heat budget terms in Southern Ocean: OHS (black), OHU (red), OHT at the boundary of the Atlantic and Southern Oceans (gold; same as the orange curve in **a**), and OHT at the boundary of the Indian and Southern Oceans (green; same as the green curve in **b**), and OHT at the boundary of the Pacific and Southern Oceans (blue; same as the blue curve in **c**). For a basin, a positive OHT indicates an oceanic heat import while a negative OHT indicates an oceanic heat export

with neglectable interbasin ocean heat exchanges, *OHU* dominates the *OHS* within the Atlantic basin at a rate of 0.07 PW (Fig. 4a). The spatial pattern of *OHC* trend generally follows that of *NSHF* change while the latter features an increase spreading most of the Atlantic and peaking at a rate of 10 W/m² in the subpolar region (Fig. 3b). Correspondingly, the zonal mean ocean temperature exhibits a broad warming trend in the Atlantic (Fig. 5a). To the south of 20° N, the ocean warming occurs in the upper 800 m up to 0.1 K/decade. In mid-latitudes between 40° N and 60° N, the ocean warming can even penetrate to about 3000 m in form of an equatorward tongue. Given a slight AMOC change during this period, the deep-reaching warming anomaly can be mainly attributed to surface heating and resultant warming signals carried by background ocean circulations (Winston et al. 2013).

Outside the Atlantic, Arctic sea ice loss also causes changes in surface heat flux over other ocean basins during the first 10 years. For instance, we find that Arctic sea ice loss can induce warming at the North Pacific surface via enlarged turbulent heat fluxes (Fig. 3a, Fig. S5a), which could be associated with the advection of anomalous warm air from the Arctic to the surrounding regions (Sun et al. 2018). Meanwhile, the signal of stronger natural variability such as the Pacific Decadal Oscillation or Interdecadal Pacific Oscillation may still be detectable in the Pacific even in the 10-member ensemble mean. However, unlike the Atlantic, the increase in turbulent heat fluxes over the North Pacific is largely compensated by the decreases in radiative energy fluxes there (Fig. S5b). Besides, Arctic sea ice loss brings on a turbulent heat cooling in the southern and western Pacific that acts to dampen the warming in high latitudes,

Fig. 5 (Left column) Arctic sea ice loss induced annual and zonal mean temperature trends (relative to the control) over the first 10 years in the **a** Atlantic, **b** Indian Ocean, **c** Pacific and **d** Southern Ocean. (Right column) Similar to the left column but for the temperature trends over the later 100 years



resulting in few net surface heat flux changes over the Pacific (Fig. S6c). Similarly, in the Southern Hemisphere mid- and high-latitudes, Arctic sea ice loss promotes a turbulent heat warming over the Amundsen Sea and Ross Sea but a cooling over the eastern Atlantic and Indian Ocean sectors (Fig. S5a). Thus the change in *NSHF* over the Southern Ocean is negligible when it is integrated over the whole basin (Fig. S6d). Our result shows that, despite surface warming and cooling over a global scale due to rapid atmosphere processes, the basin integrated *OHU* increase is mainly confined in the Atlantic within the first 10 years after Arctic sea ice loss (Fig. S6a).

4 The slow response dominated by interbasin ocean heat exchanges

4.1 Ocean heat uptake and redistribution within the Atlantic

Arctic sea ice loss can affect global ocean heat content via oceanic processes on a multidecadal to centennial timescale by altering ocean circulations and interbasin ocean heat exchanges. In the Atlantic, the AMOC has weakened by about 6 Sv about 100 years after the sea ice

perturbation. This AMOC weakening modifies the interbasin ocean heat exchanges between the Atlantic and other oceans.

Here we decompose the \overline{OHT} change into the circulation anomaly driven component (\overline{OHT}_v') and the temperature anomaly driven component (\overline{OHT}_θ'). We find that the weakened AMOC diminishes the northward \overline{OHT}_v' by about 0.12 PW across the boundary between the Atlantic and Southern Oceans (Fig. 6b). The \overline{OHT}_v' reduction is slightly compensated by an \overline{OHT}_θ' increase (Fig. 6b) due to the enlarged vertical ocean temperature contrast such that the interbasin exchange \overline{OHT} induced by Eulerian-mean flows abates by about 0.12 PW (Fig. 6b). On the other hand, ocean eddies and diffusion processes have a minor contribution to the change in the meridional ocean heat transport here. As a result, the net northward \overline{OHT} reduces by about 0.13 PW (Fig. 6a), indicating that the Atlantic is exporting heat across the boundary between the Atlantic and Southern Oceans. Meanwhile, the northward \overline{OHT} also decreases across the boundary between the Atlantic and Arctic Oceans but by much smaller amplitude, around 0.01 PW (Fig. 4a).

Besides the \overline{OHT} changes across the Atlantic boundaries, we examine the \overline{OHU} changes within the Atlantic 100 years after the sea ice perturbation. The weakened AMOC brings down the northward ocean heat transport and hence leads to an anomalous ocean heat divergence in the subpolar North Atlantic, which in turn can modify surface heat fluxes as well as \overline{OHU} (Liu and Fedorov 2019; Liu et al. 2020). In response to Arctic sea ice loss, the AMOC slowdown produces a robust SST cooling in the North Atlantic over the “warming hole” region up to -0.6 K (Fig. 7b; also c.f. Deser et al. 2015; Simon et al. 2021; Sun et al. 2018), which enhances the atmosphere–ocean surface temperature contrast (Fig. S7b). The enlarged temperature contrast can alter the turbulent feedback via the thermal adjustment of atmosphere boundary layer to the SST anomaly and modifying the upper limit of the feedback (Hausmann et al. 2016; Zhang and Cooke 2020). This process promotes a further increase of turbulent heat fluxes and \overline{OHU} (Fig. S5g and 3e), allowing more atmospheric heat to enter the North Atlantic (e.g., Drijfhout 2015; Ma et al. 2020; Marshall and Zanna 2014; Shi et al. 2018; Winton et al. 2013).

Combining both changes in \overline{OHU} and \overline{OHT} , we find that atmospheric heat entering the subpolar North Atlantic is mostly exported into the Southern Ocean along with a slowdown of the AMOC. We compare the \overline{OHU} and \overline{OHS} between the first 10 years and the last 100 years of our experiment and find that the weakened AMOC leads to an amplified \overline{OHU} in the North Atlantic up to 10 W/m 2 (Fig. 3e). On the contrary, the \overline{OHS} decreases to the north of 20° N in the North Atlantic (Fig. 3f). Consistent with this \overline{OHS} decrease, the horizontal and vertical extents of Atlantic warming reduce. Ocean warming is mainly confined between 38° N

and 45° N in the upper 1500 m during the last 100 years, with magnitude cut by about half (Fig. 5b). To the north of 45° N, the ocean warming occurred in the first 10 years is replaced by an ocean cooling extending from the surface down to the bottom (Fig. 5b). Similar ocean temperature changes have also been found in previous cases of AMOC slowdown (e.g., He et al. 2020; Liu et al. 2020), indicative of a dominant role of ocean circulation changes in controlling subsurface temperature changes in the mid-latitude and subpolar North Atlantic.

To the south of 20° N, warming signals emerge in the upper 1400 m accompanying with the AMOC slowdown (Fig. 5b). Seen from the lower limb of the Atlantic overturning at the 1000-m level (see Fig. 8c contours), warming signals propagate southward in the Atlantic following the deep western boundary and equatorial Kelvin waves (Fig. 9b). This pattern is consistent with paleoclimate observations (Weldeab et al. 2016), revealing the path of temperature anomaly propagation and the mechanisms on ocean heat redistribution and storage in the Atlantic basin (Kostov et al. 2014; Pedro et al. 2018; Zhang et al. 2018).

4.2 Heat import and redistribution in the Indian and Pacific Oceans

From previous studies (Garuba and Klinger 2016; Sun et al. 2020), the temperature signals associated with a weakened AMOC travel along the South Atlantic eastern boundary (e.g., Huang et al. 2000; Kawase 1987; Sévellec and Fedorov 2013), which can further spread into the Indian Ocean in form of a geostrophic transport response. In the Indian Ocean, these signals act to deepen the isopycnals along the western Indian Ocean and result in anomalous ocean circulation. In our experiment, we find that the anomalous ocean circulation in the Indo-Pacific is up to 2.4 Sv at its maximum, characterized by a northward transport near the surface and a southward transport in the deep ocean (Fig. 8d). The anomalous ocean circulation generates an anomalous heat transport from the Southern Ocean to the Indian Ocean. Though the circulation driven heat transport anomaly is partially compensated by a concurrent temperature driven heat transport anomaly (Fig. 6d), the Indian Ocean receives a heat import of 0.05 PW from the Southern Ocean (Fig. 6c). This means that, about two-thirds of the redistributed heat from the Atlantic remains in the Southern Ocean, while the left one-third is imported by the Indo-Pacific after 100 years of sea ice perturbation.

The imported heat from the Atlantic is further redistributed between the Indian and Pacific Oceans by the ITF. As part of the global convey belt, the ITF also weakens, which is dynamically linked to the AMOC slowdown (Sun and Thompson 2020). The ITF weakening begins about 30 years after the Arctic sea ice perturbation, lasting for

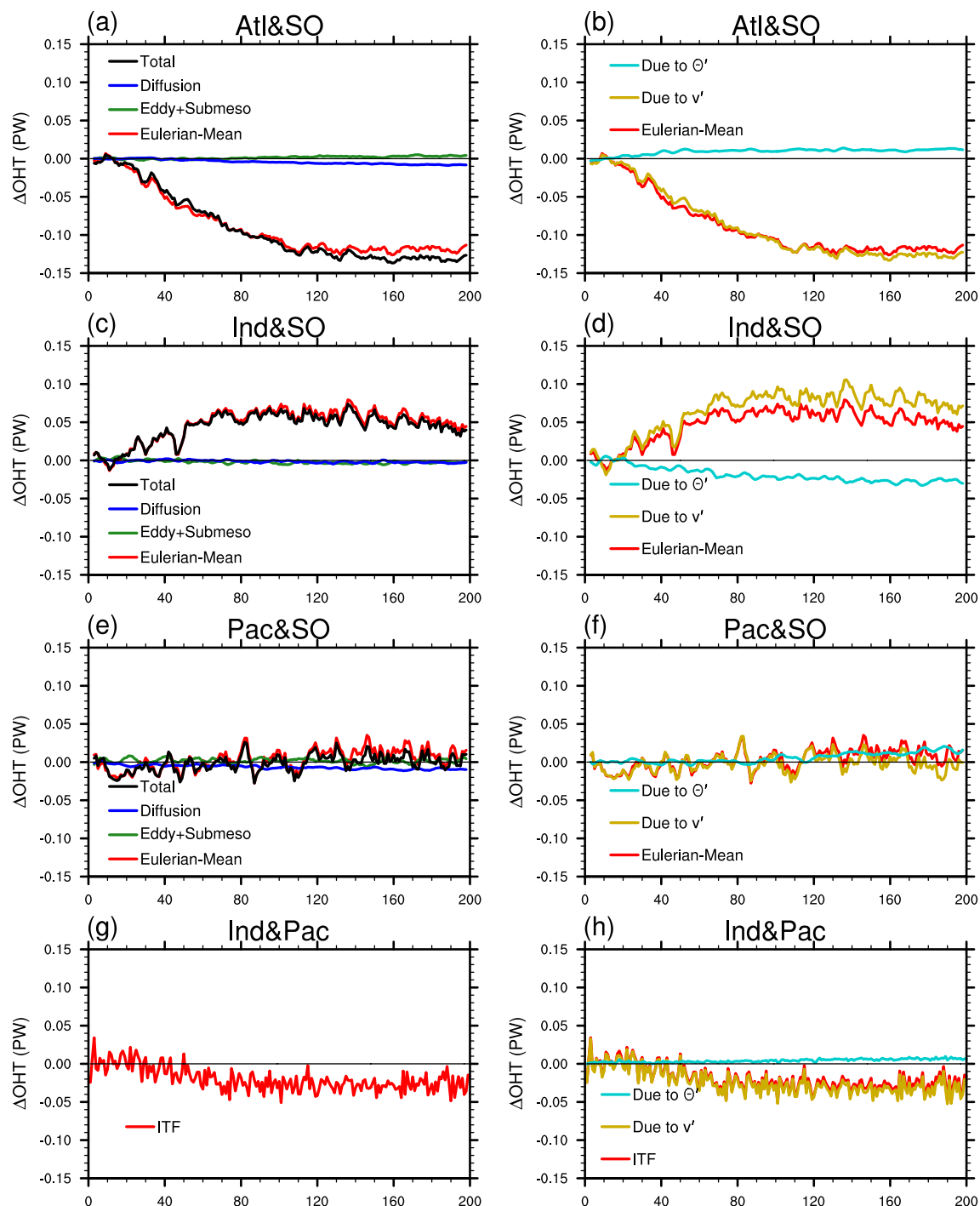


Fig. 6 **a** Arctic sea ice loss induced changes (relative to the control) in annual mean northward ocean heat transport at the boundary of the Southern and Atlantic Oceans (positive: from the Southern Ocean to the Atlantic): total (black) and the components induced by diffusion processes (blue), mesoscale and sub-mesoscale eddies (green) and Eulerian mean flow (red). **b** Replot of ocean heat transports by the Eulerian mean flow (red) in **a**, the ocean-circulation driven component (brown) and the temperature driven component (cyan). **c**, **d**: as

in **a**, **b** but for changes in annual mean northward ocean heat transport at the boundaries between the Southern and Indian Oceans and between the Southern and Pacific Oceans, respectively. **g** Changes in the ITF induced ocean heat transport (positive: from the Pacific to Indian Ocean). **h** Replot of the ITF induced heat transport (red) in **g**, the ocean-circulation driven component (brown) and the temperature driven component (cyan)

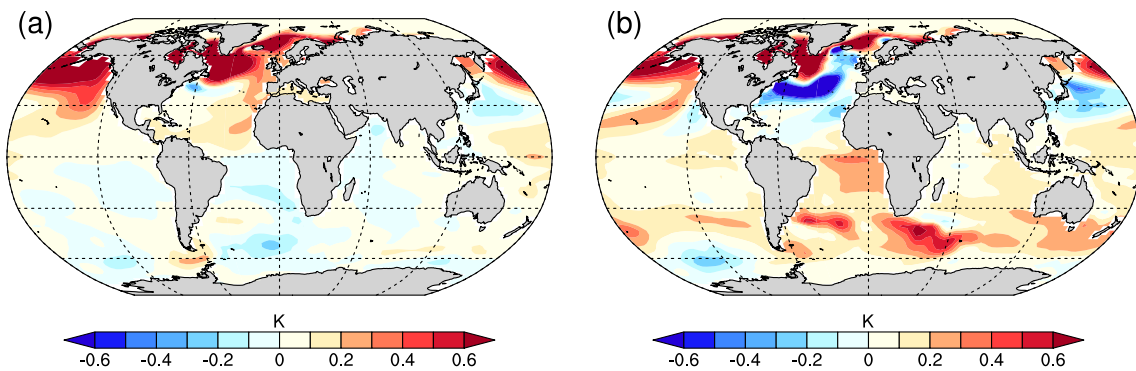


Fig. 7 Changes in sea surface temperature (SST, relative to the control) for the ensemble mean of the Arctic sea ice perturbation simulation during **a** the first 10 years and **b** the later 100 years

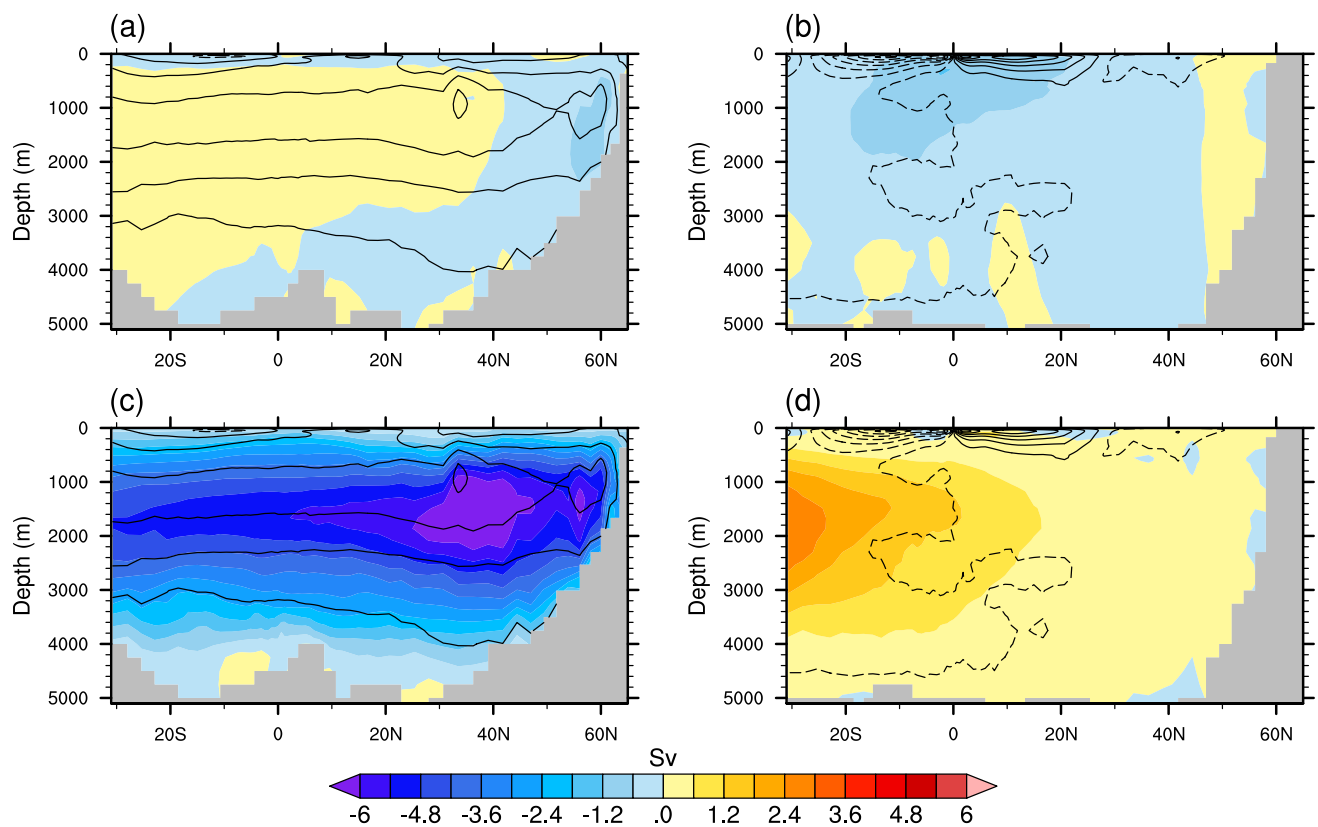


Fig. 8 (Left column) Arctic sea ice loss induced changes (relative to the control) in annual mean AMOC in the Atlantic over **a** the first 10 years and **c** the later 100 years. (Right column) As in the left column but the MOC changes in the Indo-Pacific Ocean. Annual mean

MOC climatology from control run in each ocean basin is shown in each panel [contours in Sv, with a contour interval of 5 Sv, zero contours thickened and solid (dashed) contours indicating positive (negative) values]

another 80 years and ends up with a reduction of about 1.5 Sv (Fig. 2c).

Associated with the weakened ITF, the climatological heat transport from the Pacific to the Indian Ocean is reduced by about 0.03 PW (Fig. 6g), accounting for about 60% of the imported heat into the Indian Ocean across the

boundary between the Indian and Southern Oceans. This means that the Indian Ocean imports heat from the Southern Ocean and exports part of the heat to the Pacific. As a result, about 40% of the imported heat remains in the Indian Ocean, a part of which is then released back to the atmosphere in the form of negative OHU through turbulent and radiative

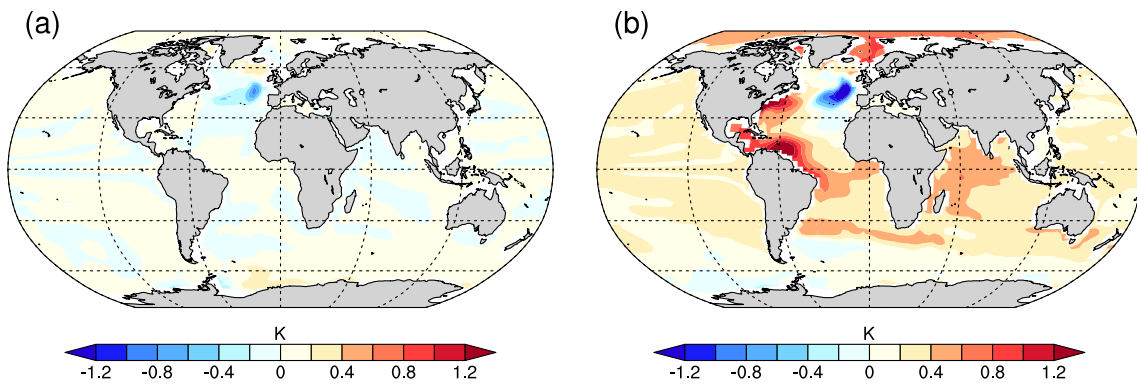


Fig. 9 Changes in ocean temperature (relative to the control) at the 1000-m level over **a** the first 10 years and **b** the last 100 years

heat fluxes (Fig. 4b). Consequently, the Indian Ocean gains heat at about 0.01 PW in response to Arctic sea ice loss as reflected by a warming trend (> 0.02 K/decade) in the upper 1000-m ocean (Fig. 5d). The anomalous heat transport associated with the weakened ITF contributes to the ocean warming in the Pacific. With small amounts of the interbasin exchanges at the boundary between the Pacific and Southern Oceans and the boundary between the Pacific and Arctic Oceans (Fig. 4c), the ITF plays a dominant role in the interbasin ocean heat transport for the Pacific basin. The changes in the ITF and associated *OHT* lead to an *OHS* increase of about 0.02 PW (Fig. 4c) that is reflected by a warming trend in the upper 800 m to the south of 40° N in the Pacific Ocean (Fig. 5f).

4.3 Linkage to the Southern Ocean

The ocean heat redistribution in the Southern Ocean is linked to both atmospheric and oceanic processes. In response to the AMOC slowdown and associated reduction of the northward ocean heat transport, the Southern Hemisphere atmosphere warms, especially in the lower to middle troposphere at high latitudes and the upper troposphere at low latitudes (Fig. S4c, also c.f. Chen et al. 2019; Deser et al. 2015). This atmospheric warming pattern is along with a southward migration of the Hadley Cell, a weakening of the northern margin of the subtropical jet as well as a poleward intensification of mid-latitude westerly winds (Fig. S4d; also c.f. Lee et al. 2011; Pedro et al. 2018). The atmospheric wind response can extend down to ocean surface and consequently modulate the wind-driven ocean circulation in the Southern Ocean. Particularly, the Southern Hemisphere westerly winds generate a northward Ekman transport, which piles waters to the north of wind maximum, combined with a downward Ekman pumping to the north of the Antarctic Circumpolar Current and a southward return flow in deep ocean, thus creating a clockwise meridional

overturning circulation (MOC) known as the so-called Deacon Cell (Döös and Webb 1994; Döös et al. 2008).

In our experiment, we find that Arctic sea ice loss induces a dipole-like pattern of surface zonal wind stress change, with positive (negative) anomalies to the south (north) of 42° S. The positive surface zonal wind stress anomalies peak around 55° S up to about 0.004 N/m 2 (Fig. 10b). Consequently, the Deacon Cell is poleward displaced and strengthened by about 0.6 Sv at its maximum (Fig. 10b), which is partially amplified (offset) by the eddy-driven MOC to the north (south) of 45° S due to altered isopycnal tilting and baroclinicity (Fig. 10d). Therefore, changes in the residual MOC generally follow those in the Deacon Cell showing a poleward shift in the later 100 years in the perturbation experiment (Fig. 10f).

Changes in the Southern Ocean MOCs are responsible for the altered *OHT* across the boundaries between the Southern Ocean and other basins (the Atlantic and the Indo-Pacific). Different from the first 10 years when the wind driven ocean circulation anomalies are mainly confined to the south of 40° S (Fig. 10a), negative surface wind stress anomaly engenders a southward flow near the surface at these boundaries in the later 100 years (Fig. 10b), therefore leading to a net *OHT* import at about 0.08 PW into the Southern Ocean. Specifically, the Southern Ocean imports about 0.13 PW from the Atlantic but exports about 0.05 PW to the Indian Ocean (Fig. 4d). Meanwhile, the Southern Ocean releases heat of about 0.03 PW via ocean surface back to the atmosphere primarily via diminished turbulent heat fluxes (Fig. S6d). As a result, the basin-integrated *OHS* is increased by about 0.05 PW (Fig. 4d), which indicates a subsurface warming and an *OHC* increase within the Southern Ocean.

We further find that Arctic sea ice loss induced Southern Ocean warming mainly occurs to the north of 50° S manifesting a downward and equatorward warming tongue (> 0.02 K/decade) to the north of 47° S (Fig. 5h). Our result well agrees with Pedro et al. (2018) and suggests that the Southern Ocean plays an important role in global

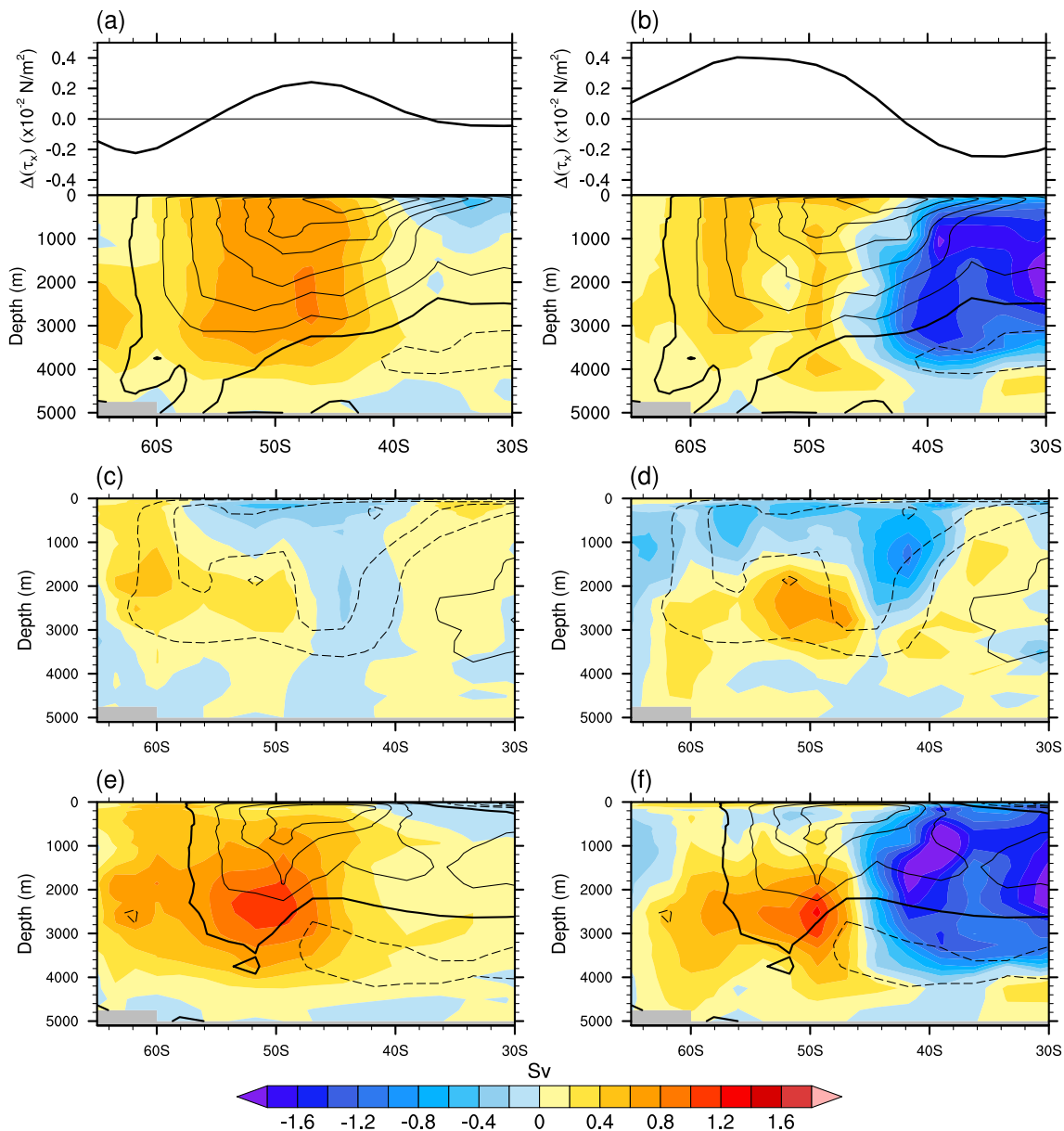


Fig. 10 (Left column) Arctic sea ice loss induced changes (relative to the control) in annual mean **a** Eulerian mean, **c** eddy-induced, and **e** residual MOCs (shading in Sv) in the Southern Ocean during the first 10 years. (Right column) As in the left column but the MOC changes during the last 100 years. Annual mean MOC climatology from control run is shown in each panel [contours in Sv, with a contour inter-

val of 5 Sv, zero contours thickened and solid (dashed) contours indicating positive (negative) values]. Arctic sea ice loss induced changes (relative to the control) in annual and zonal mean zonal surface wind stress curl during the first 10 years and the last 100 years in the experiment are attached on **a** and **b**, respectively

ocean heat redistribution. The region to the north of the Antarctic Circumpolar Current serves as a heat reservoir, whilst the region to the south is seldom involved. Two processes operate during the interbasin heat redistribution. On one hand, triggered by the Arctic sea ice loss, the poleward intensified Southern Hemisphere westerly winds enhance the Ekman downwelling in the mid-latitude ocean, deepen the isopycnals and bring on a subsurface warming (e.g., Li et al. 2021a, b; Liu et al. 2018; Lyu et al. 2020). On the

other hand, Arctic sea ice loss results in a “mini” global warming along with a significant surface warming in the mid- and high-latitude Southern Ocean (Fig. 7b). The subduction of the surface warming signals can also contribute to the warming in the interior ocean (e.g., Lyu et al. 2020). Both processes highlight the important role of the atmosphere–ocean coupling and teleconnection in understanding the global effects of Arctic sea ice loss.

5 Conclusion and discussions

In this study, we analyze the effects of Arctic sea ice loss on global ocean circulation changes and global heat redistribution by conducting ensemble sea ice perturbation simulations with a fully coupled climate model. We find that Arctic sea ice loss promotes ocean heat uptake in the North Atlantic “warming hole” region via an increase of turbulent heat fluxes. During the first 10 years since sea ice perturbation, the AMOC is little altered such as most of the taken heat is stored locally in the Atlantic. However, after the first decade, the AMOC starts to weaken, which effectively redistributes most of the taken heat from the atmosphere to other ocean basins. Meanwhile, In the Indo-Pacific Ocean, an anomalous ocean circulation is generated in the Indo-Pacific Oceans appearing as an abnormal northward flow near the surface. This anomalous ocean circulation carries about one-third of the redistributed heat from the Atlantic to the Indian Ocean. The ITF that connects the Indian and Pacific Oceans also weakened in response to Arctic sea ice loss, which reduces the climatological ocean heat transport from the Pacific to Indian Ocean and consequently acts to warm the Pacific but cool the Indian Ocean. As a result, either the Indian or Pacific Ocean has a net import of oceanic heat from other basins as well an increase of basin-integrated *OHS*. In the Southern Ocean, Arctic sea ice loss induces a strong warming in the low troposphere peaking around 50° S, which further weakens the equatorward flank of the westerly winds. This wind change modifies the MOCs in the Southern Ocean and causes an anomalous southward flow at the boundary between the Southern Ocean and Atlantic/ Indo-Pacific Oceans. As a result, about two-thirds of the redistributed heat from the Atlantic remains in the Southern Ocean and lead to an interior ocean warming.

Our results have great implications on global ocean heat redistributions in future and past climate changes considering that an AMOC slowdown can occur in either scenario. For example, the Southern Ocean warming under future anthropogenic forcing has been mostly viewed as a result of the subduction of surface warming along constant density surfaces (Church et al. 1991; Garuba and Klinger 2016; Gregory et al. 2016); or temperature anomalies carried by climatological MOCs in the Southern Ocean (Marshall et al. 2015). Nevertheless, as suggested by the results in the current study, the MOC change and circulation-driven cross-boundary *OHT* change can contribute to the Southern Ocean warming (Liu et al. 2018; Shi et al. 2020); , which, meanwhile, are inherently linked to the AMOC and its associated *OHT* changes (Pedro et al. 2018; Sun and Thompson 2020; Sun et al. 2020).

It is worth noting that the Arctic Ocean is also warming in our perturbation experiment, which is consistent with

observations (e.g., Grotfendt et al. 1998; Burgard and Notz 2017; Steele et al. 2008), suggesting that sea ice loss also plays a role in modifying the Arctic heat budget. On one hand, Arctic sea ice loss opens the atmosphere–ocean interface and thus facilitates more solar energy flux into the ocean (Liu et al. 2019). Sea ice melting itself meanwhile can also directly alter the heat flux over the surface of the Arctic Ocean. On the other hand, the ocean heat transports across the boundaries between the Arctic and North Atlantic/Pacific Oceans will be modified as a result of the global impacts of Arctic sea ice loss on ocean circulations and interbasin heat exchanges (Fig. 4a, c, also c.f. Liu and Fedorov 2021; Li et al. 2021). Both changes in surface heat flux and inter-basin ocean heat transport act to modulate the ocean heat budget in the Arctic Ocean.

It also merits attention that a recent AMOC reconstruction at 26° N based on satellite altimetry and cable measurements suggests an AMOC decline during 1993–2014, and the decline is especially robust since mid-2000s (Frajka-Williams 2015). The observed Arctic sea ice loss since the satellite era could have been playing a role, whereas many other factors such as greenhouse gases (e.g., Gregory et al. 2005) and aerosol (e.g., Hassan et al. 2021) changes and even natural climate variability (Robert et al. 2014) could contribute to this observed AMOC change as well.

Supplementary Information The online version contains supplementary material available at <https://doi.org/10.1007/s00382-022-06241-0>.

Acknowledgements This work is supported by U.S. National Science Foundation (AGS-2053121, OCE 2123422). W.L. has also been supported by the Alfred P. Sloan Foundation as a Research Fellow.

Data availability The NSIDC observation data of Arctic sea ice concentration and extent are available at <https://nsidc.org/>. The CESM Arctic sea ice perturbation experiment data are available on request from the corresponding author.

References

- Bakker P, Schmittner A, Lenaerts JT, Abe-Ouchi A, Bi D, van den Broeke MR, Chan WL, Hu A, Beadling RL, Marsland SJ, Mernild SH (2016) Fate of the Atlantic meridional overturning circulation: strong decline under continued warming and Greenland melting. *Geophys Res Lett* 43:252–260
- Burgard C, Notz D (2017) Drivers of Arctic Ocean warming in CMIP5 models. *Geophys Res Lett* 44:4263–4271
- Cessi P, Bryan K, Zhang R (2004) Global seiching of thermocline waters between the Atlantic and the Indian-Pacific Ocean Basins. *Geophys Res Lett* 31:L04302
- Chen C, Liu W, Wang G (2019) Understanding the uncertainty in the 21st century dynamic sea level projections: the role of the AMOC. *Geophys Res Lett* 46:210–217
- Chiang JC, Bitz CM (2005) Influence of high latitude ice cover on the marine intertropical convergence zone. *Clim Dyn* 25:477–496

Church JA, Godfrey JS, Jackett DR, McDougall TJ (1991) A model of sea level rise caused by ocean thermal expansion. *J Clim* 4:438–456

Deser C, Tomas R, Alexander M, Lawrence D (2010) The seasonal atmospheric response to projected Arctic sea ice loss in the late twenty-first century. *J Clim* 23:333–351

Deser C, Tomas RA, Sun L (2015) The role of ocean–atmosphere coupling in the zonal-mean atmospheric response to Arctic sea ice loss. *J Clim* 28:2168–2186

Ding Q, Schweiger A, L'Heureux M, Battisti DS, Po-Chedley S, Johnson NC, Blanchard-Wrigglesworth E, Harnos K, Zhang Q, Eastman R, Steig EJ (2017) Influence of high-latitude atmospheric circulation changes on summertime Arctic sea ice. *Nat Clim Change* 7:289–295

Döös K, Webb DJ (1994) The Deacon cell and the other meridional cells of the Southern Ocean. *J Phys Oceanogr* 24:429–442

Döös K, Nylander J, Coward AC (2008) Lagrangian decomposition of the Deacon Cell. *J Geophys Res* 113:C07028

Drijfhout SS (2015) Global radiative adjustment after a collapse of the Atlantic meridional overturning circulation. *Clim Dyn* 45:1789–1799

Frajka-Williams E (2015) Estimating the Atlantic overturning at 26°N using satellite altimetry and cable measurements. *Geophys Res Lett* 42:3458–3464

Francis JA, Chan W, Leathers DJ, Miller JR, Veron DE (2009) Winter Northern Hemisphere weather patterns remember summer Arctic sea-ice extent. *Geophys Res Lett* 36:L07503

Garuba OA, Klinger BA (2016) Ocean heat uptake and interbasin transport of the passive and redistributive components of surface heating. *J Clim* 29:7507–7027

Gent PR, Danabasoglu G (2011) Response to increasing Southern Hemisphere winds in CCSM4. *J Clim* 24:4992–4998

Gent PR, McWilliams JC (1990) Isopycnal mixing in ocean circulation models. *J Phys Oceanogr* 20:150–155

Gregory JM et al (2005) A model intercomparison of changes in the Atlantic thermohaline circulation in response to increasing atmospheric CO₂ concentration. *Geophys Res Lett* 32:L12703

Gregory JM, Bouttes N, Griffies SM, Haak H, Hurlin WJ, Jungclaus J, Kelley M, Lee WG, Marshall J, Romanou A, Saenko OA, Stammer D, Winton M (2016) The Flux-Anomaly-Forced Model Intercomparison Project (FAFMIP) contribution to CMIP6: investigation of sea-level and ocean climate change in response to CO₂ forcing. *Geosci Model Dev* 9:3993–4017

Grotefendt K, Logemann K, Quadfasel D, Ronski S (1998) Is the Arctic Ocean warming? *J Geophys Res Oceans* 103:27679–27687

Hassan T, Allen RJ, Liu W, Randles CA (2021) Anthropogenic aerosol forcing of the Atlantic meridional overturning circulation and the associated mechanisms in CMIP6 models. *Atmos Chem Phys* 21:5821–5846

Hausmann U, Czaja A, Marshall J (2016) Estimates of air-sea feedbacks on sea surface temperature anomalies in the Southern Ocean. *J Clim* 29:439–454

He C, Liu Z, Zhu J, Zhang J, Gu S, Otto-Bliesner BL, Brady E, Zhu C, Jin Y, Sun J (2020) North Atlantic subsurface temperature response controlled by effective freshwater input in “Heinrich” events. *Earth Planet Sci Lett* 539:116247

Holland MM, Bailey DA, Briegleb BP, Light B, Hunke E (2012) Improved sea ice shortwave radiation physics in CCSM4: the impact of melt ponds and aerosols on Arctic sea ice. *J Clim* 25:1413–1430

Hu S, Sprintall J (2017) Observed strengthening of interbasin exchange via the Indonesian seas due to rainfall intensification. *Geophys Res Lett* 44:1448–1456

Huang RX, Cane MA, Naik N, Goodman P (2000) Global adjustment of the thermocline in response to deepwater formation. *Geophys Res Lett* 27:759–762

Jackson LC, Wood RA (2020) Fingerprints for early detection of changes in the AMOC. *J Clim* 33:7027–7044

Johnson HL, Marshall DP (2002) A theory for the surface Atlantic response to thermohaline variability. *J Phys Oceanogr* 32:1121–1132

Jungclaus JH, Haak H, Latif M, Mikolajewicz U (2005) Arctic–North Atlantic interactions and multidecadal variability of the meridional overturning circulation. *J Clim* 18:4013–4031

Kawase M (1987) Establishment of deep ocean circulation driven by deep-water production. *J Phys Oceanogr* 17:2294–2317

Kostov Y, Armour KC, Marshall J (2014) Impact of the Atlantic meridional overturning circulation on ocean heat storage and transient climate change. *Geophys Res Lett* 41:2108–2116

Lawrence DM, Oleson KW, Flanner MG, Fletcher CG, Lawrence PJ, Levis S, Swenson SC, Bonan GB (2012) The CCSM4 land simulation, 1850–2005: assessment of surface climate and new capabilities. *J Clim* 25:2240–2260

Lee SY, Chiang JC, Matsumoto K, Tokos KS (2011) Southern Ocean wind response to North Atlantic cooling and the rise in atmospheric CO₂: modeling perspective and paleoceanographic implications. *Paleoceanography* 26:PA1214

Lee SK, Park W, Baringer MO, Gordon AL, Huber B, Liu Y (2015) Pacific origin of the abrupt increase in Indian Ocean heat content during the warming hiatus. *Nat Geosci* 8:445–449

Levermann A, Mignot J, Nawarath S, Rahmstorf S (2007) The role of northern sea ice cover for the weakening of the thermohaline circulation under global warming. *J Clim* 20:4160–4171

Li H, Fedorov AV (2021) Persistent freshening of the Arctic Ocean and changes in the North Atlantic salinity caused by Arctic sea ice decline. *Clim Dyn* 57:2995–3013

Li D, Zhang R, Knutson T (2018) Comparison of mechanisms for low-frequency variability of summer Arctic sea ice in three coupled models. *J Clim* 31:1205–1226

Li H, Fedorov AV, Liu W (2021a) AMOC stability and diverging response to Arctic sea ice decline in two climate models. *J Clim* 34:5443–5460

Li S, Liu W, Lyu K, Zhang X (2021b) The effects of historical ozone changes on Southern Ocean heat uptake and storage. *Clim Dyn* 22:1–7

Liu W, Fedorov AV (2019) Global impacts of Arctic sea ice loss mediated by the Atlantic meridional overturning circulation. *Geophys Res Lett* 46:944–952

Liu W, Fedorov AV (2021) Interaction between Arctic sea ice and the Atlantic meridional overturning circulation in a warming climate. *Clim Dyn*. <https://doi.org/10.1007/s00382-021-05993-5>

Liu W, Xie S-P, Liu Z, Zhu J (2017) Overlooked possibility of a collapsed Atlantic meridional overturning circulation in warming climate. *Sci Adv* 3:e1601666

Liu W, Lu J, Xie S-P, Fedorov A (2018) Southern Ocean heat uptake, redistribution, and storage in a warming climate: the role of meridional overturning circulation. *J Clim* 31:4727–4743

Liu W, Fedorov AV, Sévillec F (2019) The mechanisms of the Atlantic meridional overturning circulation slowdown induced by Arctic sea ice decline. *J Clim* 32:977–996

Liu W, Fedorov AV, Xie S-P, Hu S (2020) Climate impacts of a weakened Atlantic Meridional overturning circulation in a warming climate. *Sci Adv* 6:eaaz4876

Lyu K, Zhang X, Church JA, Wu Q (2020) Processes responsible for the Southern Hemisphere ocean heat uptake and redistribution under anthropogenic warming. *J Clim* 33:3787–3807

Ma X, Liu W, Allen RJ, Huang G, Li X (2020) Dependence of regional ocean heat uptake on anthropogenic warming scenarios. *Sci Adv* 6:eabc0303

Marshall DP, Zanna L (2014) A conceptual model of ocean heat uptake under climate change. *J Clim* 27:8444–8465

Marshall J, Scott JR, Armour KC, Campin JM, Kelley M, Romanou A (2015) The ocean's role in the transient response of climate to abrupt greenhouse gas forcing. *Clim Dyn* 44:2287–2299

McManus JF, Francois R, Gherardi JM, Keigwin LD, Brown-Leger S (2004) Collapse and rapid resumption of Atlantic meridional circulation linked to deglacial climate changes. *Nature* 428:834–837

Neale RB et al (2010) Description of the NCAR community atmosphere model (CAM 5.0), vol 1. NCAR Tech. Note NCAR/TN-486+STR, pp 1–121

Oudar T, Sanchez-Gomez E, Chauvin F, Cattiaux J, Terray L, Cassou C (2017) Respective roles of direct GHG radiative forcing and induced Arctic sea ice loss on the Northern Hemisphere atmospheric circulation. *Clim Dyn* 49:3693–3713

Overland JE, Wang M (2010) Large-scale atmospheric circulation changes are associated with the recent loss of Arctic sea ice. *Tellus A Dyn Meteorol Oceanogr* 62:1–9

Park HS, Lee S, Son SW, Feldstein SB, Kosaka Y (2015) The impact of poleward moisture and sensible heat flux on Arctic winter sea ice variability. *J Clim* 28:5030–5040

Pedro JB, Jochum M, Buzert C, He F, Barker S, Rasmussen SO (2018) Beyond the bipolar seesaw: toward a process understanding of interhemispheric coupling. *Quat Sci Rev* 192:27–46

Peings Y, Magnusdottir G (2014) Response of the wintertime Northern Hemisphere atmospheric circulation to current and projected Arctic sea ice decline: a numerical study with CAM5. *J Clim* 27:244–264

Rinke A, Dethloff K, Dorn W, Handorf D, Moore JC (2013) Simulated Arctic atmospheric feedbacks associated with late summer sea ice anomalies. *J Geophys Res Atmos* 118:7698–7714

Roberts CD, Jackson L, McNeall D (2014) Is the 2004–2012 reduction of the Atlantic meridional overturning circulation significant? *Geophys Res Lett* 41:3204–3210

Screen JA, Simmonds I (2010) The central role of diminishing sea ice in recent Arctic temperature amplification. *Nature* 464:1334–1337

Screen JA, Simmonds I, Deser C, Tomas R (2013) The atmospheric response to three decades of observed Arctic sea ice loss. *J Clim* 26:1230–1248

Sévellec F, Fedorov AV (2013) The leading, interdecadal eigenmode of the Atlantic meridional overturning circulation in a realistic ocean model. *J Clim* 26:2160–2183

Sévellec F, Fedorov AV (2015) Optimal excitation of AMOC decadal variability: links to the subpolar ocean. *Prog Oceanogr* 132:287–304

Sévellec F, Fedorov AV, Liu W (2017) Arctic sea-ice decline weakens the Atlantic meridional overturning circulation. *Nat Clim Change* 7:604–610

Shi JR, Xie SP, Talley LD (2018) Evolving relative importance of the Southern Ocean and North Atlantic in anthropogenic ocean heat uptake. *J Clim* 31:7459–7479

Shi JR, Talley LD, Xie S-P, Liu W, Gille ST (2020) Effects of buoyancy and wind forcing on Southern Ocean climate change. *J Clim* 33:10003–10020

Simon A, Gastineau G, Frankignoul C, Rousset C, Codron F (2021) Transient climate response to Arctic sea ice loss with two ice-constraining methods. *J Clim* 34:3295–3310

Smith R, Jones P, Briegleb B, Bryan F, Danabasoglu G, Dennis J, Hecht M (2010) The parallel ocean program (POP) reference manual: ocean component of the community climate system model (CCSM) and community earth system model (CESM). In: LAUR-01853, 141:1–140

Steele M, Ermold W, Zhang J (2008) Arctic Ocean surface warming trends over the past 100 years. *Geophys Res Lett* 35:L02614

Stroeve JC, Kattsov V, Barrett A, Serreze M, Pavlova T, Holland M, Meier WN (2012) Trends in Arctic sea ice extent from CMIP5, CMIP3 and observations. *Geophys Res Lett* 39:L16502

Sun S, Thompson AF (2020) Centennial changes in the Indonesian Throughflow connected to the Atlantic Meridional Overturning Circulation: the ocean's transient conveyor belt. *Geophys Res Lett* 47:e2020GL090615

Sun L, Alexander M, Deser C (2018) Evolution of the global coupled climate response to Arctic sea ice loss during 1990–2090 and its contribution to climate change. *J Clim* 31:7823–7843

Sun S, Thompson AF, Eisenman I (2020) Transient overturning compensation between Atlantic and Indo-Pacific basins. *J Phys Oceanogr* 50:2151–2172

Vihma T (2014) Effects of Arctic sea ice decline on weather and climate: a review. *Surv Geophys* 35:1175–1214

Weldeab S, Friedrich T, Timmermann A, Schneider RR (2016) Strong middepth warming and weak radiocarbon imprints in the equatorial Atlantic during Heinrich 1 and Younger Dryas. *Paleoceanography* 31:1070–1082

Winton M, Griffies SM, Samuels BL, Sarmiento JL, Frölicher TL (2013) Connecting changing ocean circulation with changing climate. *J Clim* 26:2268–2278

Yang H, Zhao Y, Liu Z, Li Q, He F, Zhang Q (2015a) Heat transport compensation in atmosphere and ocean over the past 22,000 Years. *Sci Rep* 5:16661

Yang H, Li Q, Wang K, Sun Y, Sun D (2015b) Decomposing the meridional heat transport in the climate system. *Clim Dyn* 44:2751–2768

Zhang R (2010) Latitudinal dependence of Atlantic meridional overturning circulation (AMOC) variations. *Geophys Res Lett* 37:L16703

Zhang L, Cooke W (2020) Simulated changes of the Southern Ocean air-sea heat flux feedback in a warmer climate. *Clim Dyn* 22:1–16

Zhang R, Delworth TL (2005) Simulated tropical response to a substantial weakening of the Atlantic thermohaline circulation. *J Clim* 18:1853–1860

Zhang M, Wu Z, Qiao F (2018) Deep Atlantic Ocean warming facilitated by the deep western boundary current and equatorial Kelvin waves. *J Clim* 31:8541–8555

Publisher's Note Springer Nature remains neutral with regard to jurisdictional claims in published maps and institutional affiliations.